Entropy hysteresis and nonequilibrium thermodynamic efficiency of ion conduction in a voltage-gated potassium ion channel

Biswajit Das, Kinshuk Banerjee, and Gautam Gangopadhyay*
S. N. Bose National Centre For Basic Sciences Block JD, Sector III, Salt Lake, Kolkata 700098, India
(Received 14 July 2012; revised manuscript received 16 October 2012; published 27 December 2012)

Here we have studied the nonequilibrium thermodynamic response of a voltage-gated *Shaker* potassium ion channel using a stochastic master equation. For a constant external voltage, the system reaches equilibrium indicated by the vanishing total entropy production rate, whereas for oscillating voltage the current and entropy production rates show dynamic hysteretic behavior. Here we have shown quantitatively that although the hysteresis loop area vanishes in low and high frequency domains of the external voltage, they are thermodynamically distinguishable. In the very low frequency domain, the system remains close to equilibrium, whereas at high frequencies it goes to a nonequilibrium steady state (NESS) associated with a finite value of dissipation function. At NESS, the efficiency of the ion conduction can also be related with the nonlinear dependence of the dissipation function on the power of the external field. Another intriguing aspect is that, at the high frequency limit, the total entropy production rate oscillates at NESS with half of the time period of the external voltage.

DOI: 10.1103/PhysRevE.86.061915 PACS number(s): 87.16.Vy, 05.70.Ln, 05.10.Gg, 05.90.+m

I. INTRODUCTION

The study of ion channels plays an important role in understanding the propagation of nerve impulse and a wide variety of phenomena associated with excitable tissue of neural as well as non-neural nature [1–4]. Ion channels maintain a controlled exchange of ions between the cells and the extracellular medium through ion-permeable pores with the rearrangement of the tertiary structure of channel proteins. A great deal of understanding about the function of ion channels owes its origin in the experiments using the voltage clamp method [3–11]. In a traditional voltage clamp technique, ion flow across a cell membrane is measured as electric current, while the membrane voltage is held under experimental control with a feedback circuit [3–8]. Current due to a single ion channel can also be measured using a patch clamp experiment based on a similar principle [4]. Recently, nonequilibrium response spectroscopy [12,13] has added a new dimension in the field of ion channel experiments using the oscillating-voltage protocol. This technique has been used for the selection of an appropriate Markov model from various possible schemes of ion channel kinetics [12–16]. From kinetic studies, it has been found qualitatively that the oscillating voltage drives the ion channel out of equilibrium and resists the system to relax back to equilibrium [12–15]. The oscillating-voltage protocol [16] thus offers an opportunity to explore nonequilibrium response properties of the ion channel such as hysteresis [17] at nonequilibrium steady state (NESS).

Hysteresis has a long history [17] in its wide manifestation in various magnetic [18,19] and other condensed-matter systems [20,21] as well as in biological processes [16,22,23]. In voltage-gated ion channels, hysteresis can occur when the time period of the oscillating external voltage is comparable to the characteristic relaxation time of the conformational transitions between conducting and nonconducting states [23–26]. The channel hysteresis has biological relevance; for example, it plays an important functional role in regulating physiological phenomena and is also a governing factor in maintaining the action of a neuron pacemaker [25]. A detailed theoretical description of hysteresis in ion channel for oscillating voltage was given by Pustovoit *et al.* [26] by considering a simple two-state model. Recently, Andersson described the hysteresis of ionic conductance [27] for oscillating voltage by considering the analysis of Pustovoit *et al.* [26] and then they have extended the study of the channel gating schemes for multiple states with independent as well as cooperative gating. Their studies [26,27] reveal that the probability-voltage as well as the current-voltage hysteresis is dynamic in nature. The hysteresis loop area vanishes at the low and high frequency limits of the external oscillating voltage due to the wide time scale separation. Now, particularly for time-dependent external voltage, the system can go arbitrarily far away from equilibrium. Hence, along with the kinetic properties, the nonequilibrium thermodynamic features of the ion channel must also be explored. In this perspective, we have raised the following questions. (i) Are these low and high frequency limiting situations equivalent from the thermodynamic viewpoint or does the vanishing of an out-of-equilibrium phenomenon like hysteresis ensure that the system is at thermodynamic equilibrium? (ii) At NESS, how is the supplied energy utilized for the production of ionic current? To address the above issues coherently, we present a detailed nonequilibrium thermodynamic analysis of a voltage-gated *Shaker* potassium ion channel. The ion channel kinetics is described by a master equation constructed on the basis of the best-suited Markov process proposed in an experimental work [14]. Starting from a model consisting of five states, we have discussed about how the stochastic conformational states are connected with the essential features of a traditional Hodgkin-Huxley equation at a constant voltage. We then have explored the nonequilibrium thermodynamic features due to oscillating voltage.

The paper is organized as follows. In Sec. II A, we describe the kinetic scheme which is efficient to describe the ion channel kinetics both for constant and oscillating voltages [14]. For

*gautam@bose.res.in

the constant-voltage case, we discuss the Hodgkin-Huxley equation for the probability of the ion-conducting state. In Sec. II C, the case of time-dependent voltage is considered, where we give the analytical expression of the probability of the ion-conducting state. Expressions of total, medium, and system entropy production rates are given in Sec. II D for the nonequilibrium characterization of the system. In Sec. III we determine the various entropy production rates as well as the ionic current for constant and oscillating voltages and study the hysteretic behavior to characterize the nonequilibrium response properties of the system. In the discussion section we have extended the kinetic results of the single ion channel for a finite number of ion channels. Finally, the paper is concluded in Sec. IV.

II. MARKOV MODEL OF A VOLTAGE-GATED POTASSIUM ION CHANNEL: ENTROPY PRODUCTION OF THE CHANNEL KINETICS

In this section, first, we provide the master equation describing the voltage-gated potassium ion channel kinetics. For the constant-voltage case, the connection of the master equation with the Hodgkin-Huxley equation and results of the probability of ion-conduction are discussed. The time-dependent solution of the ion-conducting state probability is then given for oscillating voltage for a five-state model with one conducting and four nonconducting states. The corresponding expressions of the system, medium, and total entropy production rates then are provided.

A. Kinetic scheme of potassium ion channel and the master equation

Various experimental results reveal that a potassium ion channel is composed of four independent homologous subunits [28–30], where each subunit remains in several conformational states. For simplicity, we consider only two conformational states of each subunit, i.e., inactive and active [31–33]. The dynamics of the potassium channel can be described in terms of the number of subunits in active state at a particular instant of time. An optimum kinetic scheme of the activation of a voltage-gated potassium ion channel [6,14] can be written as

$$C_0 \underset{k_{-1}(V(t))}{\overset{4k_1(V(t))}{\rightleftharpoons}} C_1 \underset{2k_{-1}(V(t))}{\overset{3k_1(V(t))}{\rightleftharpoons}} C_2 \underset{3k_{-1}(V(t))}{\overset{2k_1(V(t))}{\rightleftharpoons}} C_3 \underset{4k_{-1}(V(t))}{\overset{k_1(V(t))}{\rightleftharpoons}} C_4, \tag{1}$$

where C_n represents the n-th conformational state of the ion channel with n number of subunits in active state with $n = 0,1,\ldots 4$. The number of subunits in the active state can increase or decrease by one unit due to the occurrence of a forward or a backward reaction with voltage-dependent rate constants, $k_1(V(t))$ and $k_{-1}(V(t))$, respectively. Here $V(t)$ is the time-dependent external voltage. The rate constants are explicitly defined as [14]

$$k_1(V(t)) = k_1(0)\exp\left[\frac{q^+V(t)}{k_BT'}\right]$$

and

$$k_{-1}(V(t)) = k_{-1}(0)\exp\left[\frac{q^-V(t)}{k_BT'}\right], \tag{2}$$

where $q^{\pm}$ are the gating charges associated with each forward and backward transition, respectively. $k_1(0)$ and $k_{-1}(0)$ are the forward and backward rate constants at zero voltage, T' is the absolute temperature, and k_B is the Boltzmann constant. During the time evolution, the number of subunits in the active state becomes a fluctuating quantity [34–36] for a single ion channel. Therefore, the system performs a one-dimensional random walk along these dynamical states [34,35]. The state C_4 is considered the ion-conducting state where all the subunits are simultaneously in the active state. To describe the time evolution of the single ion channel, we have constructed a stochastic master equation [32,36–38] in terms of the number of subunits in active state at a particular instant of time, t. The master equation can be written as

$$\frac{dP_n(t)}{dt} = \sum_{\mu=\pm1}[w_\mu(n-\nu_\mu|n)(t)P_{(n-\nu_\mu)}(t) - w_{-\mu}(n|n-\nu_\mu)(t)P_n(t)], \tag{3}$$

where ν_μ is the stoichiometric coefficient of the μ-th reaction and $\nu_1 = 1$ for the forward process and $\nu_{-1} = -1$ for the backward process. $P_n(t)$ is the probability of having n number of subunits in active state at time t where n runs from 0 to n_T. Here n_T is the total number of subunits with $n_T = 4$. The forward process, say $\mu = 1$, transforms the state $(n-1)$ to n and the reverse process, $\mu = -1$, transforms the state n to $(n-1)$. The corresponding transition probabilities are defined as

$$w_1(n-1|n)(t) = k_1(V(t))[n_T - (n-1)]$$

and

$$w_{-1}(n|n-1)(t) = k_{-1}(V(t))(n). \tag{4}$$

Now putting the transition probabilities in Eq. (3), we obtain the simplified form of the master equation as

$$\frac{dP_n(t)}{dt} = k_1(V(t))(n_T - n + 1)P_{(n-1)}(t) + k_{-1}(V(t))(n+1)P_{(n+1)}(t) - k_1(V(t))(n_T - n)P_n(t) - k_{-1}(V(t))nP_n(t). \tag{5}$$

B. Constant-voltage case: Hodgkin-Huxley results from the master equation

Traditionally the ion channel kinetics is studied using the voltage clamp technique, where the voltage is varied, say, from one holding potential to another by matching the voltage value to a variable control voltage [6–8,27]. Thereby the ion channel conductance relaxes towards its new equilibrium [27]. In the constant-voltage case, the solution of the master equation described in Eq. (3) becomes a binomial probability distribution function [32,34,35,39–42] given as

$$P_n(t) = \frac{n_T!}{n!(n_T-n)!}X^n(Y)^{n_T-n}. \tag{6}$$

Here

$$X(t) = \frac{k_1(V)(1-\exp\{-[k_1(V)+k_{-1}(V)]t\})}{k_1(V)+k_{-1}(V)}, \tag{7}$$

$$Y(t) = [1 - X(t)] = \frac{k_{-1}(V) + k_1(V)\exp\{-[k_1(V) + k_{-1}(V)]t\}}{k_1(V) + k_{-1}(V)}, \quad (8)$$

assuming that, initially, all the subunits are in the inactive state, C_0 i.e, the $n = 0$ state. This solution is well known for the independent conformational transitions of the ion channel subunits [32,43]. So the overall dynamics of the ion channel having $n_T = 4$ number of independent subunits can be expressed in terms of the dynamics of a single subunit described by the variables $X(t)$ and $Y(t)$. This idea has been put forward by a number of authors in the context of ion channels [32], enzyme kinetics [40,41], and receptors [42,43]. The combinatorial factor appearing in front of Eq. (6) gives the number of ways to choose n active states from n_T.

The average number of subunits in the active state is expressed as $\langle n \rangle(t) = n_T X(t)$ and the average number of subunits in the inactive state is $\langle n_T - n \rangle(t) = n_T Y(t)$. The parameter $X(t)$ satisfies the differential equation [3,32]

$$\frac{dX(t)}{dt} = k_1(V)[1 - X(t)] - k_{-1}(V)(X(t)). \quad (9)$$

This equation is identical to the equation for the "open probability" originally introduced by Hodgkin and Huxley to model the potassium ion channel conductance [3,32]. However, they did not consider the details of the conformational dynamics of the channel subunits as described here in the master equation.

Furthermore, the probability of ion conducting state, $P_{n_T}(t)$ $(n_T = 4)$, at steady state can be obtained from Eq. (6) as

$$P_{n_T}^{(\mathrm{ss})} = [X^{(\mathrm{ss})}]^{n_T}. \quad (10)$$

Here $X^{(\mathrm{ss})}$ is the steady-state value of $X(t)$ given from Eq. (7) as $X^{(\mathrm{ss})} = \frac{k_1(V)}{k_1(V)+k_{-1}(V)}$. Using the value of $X^{(\mathrm{ss})}$ in Eq. (10), we get

$$P_{n_T}^{(\mathrm{ss})} = \left[\frac{k_1(V)}{k_1(V) + k_{-1}(V)}\right]^{n_T}. \quad (11)$$

Now substituting the expressions of $k_1(V)$ and $k_{-1}(V)$ from Eq. (2) into Eq. (11), we finally obtain the steady-state probability of the ion-conducting state [6],

$$P_{n_T}^{(\mathrm{ss})} = \left\{\frac{1}{1 + K_{\mathrm{eq}}(0)\exp\left[\frac{-q(V)}{k_B T'}\right]}\right\}^{n_T}, \quad (12)$$

with $q = (q^+ - q^-)$ and where $K_{\mathrm{eq}}(0)$ is the equilibrium constant defined as $K_{\mathrm{eq}}(0) = [\frac{k_{-1}(0)}{k_1(0)}]$. The above probability is of the form of the Boltzmann distribution of power n_T, usually used for calculating the probability of ion-conducting state in voltage clamp experiments. There n_T is taken as the number of independent and identical transitions [6]. Therefore, at constant voltage, the probability of ion-conducting state becomes a powered Boltzmann distribution.

C. Solution of ion channel kinetics for oscillating voltage

Here we have described the kinetics of a single potassium ion channel for oscillating voltage based on the reaction scheme in Eq. (1). To get some analytical understanding, we have expressed the overall reaction in terms of the ion-conducting state, which is designated as C_4 in the reaction scheme. The probability rate equation for this state can be easily obtained from Eq. (3) as

$$\frac{dP_4(t)}{dt} = k_1(V(t))P_3(t) - n_T k_{-1}(V(t))P_4(t). \quad (13)$$

By using the normalization condition $\sum_{n=0}^{4} P_n(t) = 1$, we can rewrite Eq. (13) as

$$\frac{dP_4(t)}{dt} = \chi(t) - K(t)P_4(t), \quad (14)$$

where $\chi(t) = k_1(V(t))[1-\{P_0(t) + P_1(t) + P_2(t)\}]$ and $K(t) = [k_1(V(t)) + n_T k_{-1}(V(t))]$.

The solution of the above equation can be written as

$$P_4(t) = P_4(t_0)\exp\left[-\int_{t_0}^{t} K(t')dt'\right] + \int_{t_0}^{t} \chi(t')\exp\left[-\int_{t'}^{t} K(t'')dt''\right]dt'. \quad (15)$$

Using Eq. (15), one can write $P_4(t)$ for $mT < t < (m+1)T$ as [26]

$$P_4(mT + t) = P_4(mT)\exp\left[-\int_{mT}^{t} K(t')dt'\right] + \int_{mT}^{t} \chi(t') \times \exp\left[-\int_{t'}^{t} K(t'')dt''\right]dt', \quad (16)$$

where T is the time period of the oscillating voltage and m $(= 0,1,2,\ldots)$ is the index of the oscillation period. Now, using Eq. (15), one can write a recursion formula connecting the probabilities $P_4(mT)$ and $P_4[(m+1)T]$ as

$$P_4[(m+1)T] = \phi P_4(mT) + \Delta_0, \quad (17)$$

where ϕ and Δ_0 are given by

$$\phi = \exp\left[-\int_0^T K(t)dt\right] \quad (18)$$

and

$$\Delta_0 = \int_0^T \chi(t')\exp\left[-\int_{t'}^{T} K(t'')dt''\right]dt'. \quad (19)$$

The above recursion relation gives the value of $P_4(mT)$ as

$$P_4(mT) = \phi^m P_4(0) + \frac{1-\phi^m}{1-\phi}\Delta_0, \quad (20)$$

where $P_4(0)$ is the initial probability of the ion-conducting state. When $m \to \infty$, the probability $P_4(mT)$ approaches its asymptotic value,

$$\lim_{m\to\infty} P_4(mT) = \frac{\Delta_0}{1-\phi}. \quad (21)$$

By substituting the above equation into Eq. (16) and taking the asymptotic long time limit of the probability, $P_4(mT + t)$, which is denoted as $P_4^{(\mathrm{ss})}(t)$, we obtain

$$P_4^{(\mathrm{ss})}(t) = \lim_{m\to\infty} P_4(mT + t) = \frac{\Delta(t)}{1-\phi}. \quad (22)$$

Here the function $\Delta(t)$ is given by

$$\Delta(t) = \int_t^{t+T} \chi(t')\exp\left[-\int_{t'}^{t+T} K(t'')dt''\right]dt'. \quad (23)$$

At a very low frequency limit when $T \to \infty$, ϕ defined in Eq. (18) vanishes. Therefore, $P_4^{(ss)}(t)$ in Eq. (22) can be written as

$$P_4^{(ss)}(t) = \int_0^T \chi(t-t')\exp\left[-\int_0^{t'} K(t-t'')dt''\right]dt'. \quad (24)$$

As $\chi(t')$ and $K(t')$ are slowly varying functions in the low frequency limit, we can take the following approximation:

$$\chi(t-t') \approx \chi(t) - t'\dot{\chi}(t'), K(t-t'') \approx K(t) - t''\dot{K}(t'')$$

and

$$\exp\left[-\int_0^{t'} K(t-t'')\,dt''\right] \approx \left[1+\frac{1}{2}\dot{K}(t)t'^2\right]\exp[-K(t)t']. \quad (25)$$

Neglecting the term proportional to the product $\chi(t)K(t)$, we obtain

$$P_4^{(ss)}(t) \approx Q(t) - \frac{\dot{Q}(t)}{K(t)}, \quad (26)$$

where $Q(t) = \frac{\chi(t)}{K(t)}$. Then, for slowly varying voltage, $P_4^{(ss)}(t)$ finally becomes

$$P_4^{(ss)}(t) = \frac{\chi(t)}{K(t)}. \quad (27)$$

Similarly, in the high frequency limit when $T \to 0$, ϕ defined in Eq. (18) can be written as

$$\phi = 1 - T\langle K\rangle. \quad (28)$$

Here $\langle f\rangle = \frac{1}{T}\int_0^T f(t)dt$, where f can be $\chi(t)$ or $K(t)$. Hence, $P_4^{(ss)}(t)$ in Eq. (22) takes the form

$$P_4^{(ss)}(t) = \frac{1}{T\langle K\rangle}\int_t^{t+T} \chi(t')\exp\left[-\int_{t'}^{t+T} K(t'')dt''\right]dt'. \quad (29)$$

In the high frequency limit, we can take the following approximation:

$$\exp\left[-\int_{t'}^{t+T} K(t'')dt''\right] \approx 1 - \int_{t'}^{t+T} K(t'')dt''. \quad (30)$$

Using this approximation, Eq. (29) can be written as

$$P_4^{(ss)}(t) = \frac{\int_t^{t+T}\chi(t')dt' - \int_t^{t+T}\chi(t')dt'\int_{t'}^{t+T}K(t'')dt''}{\int_t^{t+T}K(t')dt'} = \frac{\langle\chi(t)\rangle}{\langle K(t)\rangle} - \delta(t). \quad (31)$$

Here we define $\delta(t) = \frac{\xi}{\int_t^{t+T}K(t')dt'}$, where $\xi = \int_t^{t+T}\chi(t')[\int_{t'}^{t+T}K(t'')dt'']dt'$. Here the limit t' varies in the range $t \leqslant t' \leqslant t+T$ and t'' varies in the range $t' \leqslant t'' \leqslant t+T$. In the double integration, ξ in the limit of $T \to 0$, one can approximate $[\int_{t'}^{t+T}K(t'')dt'']$ as $(T+t-t')K(t')$, where $0 \leqslant (T+t-t') \leqslant T$. This makes $\xi \approx T\int_t^{t+T}\chi(t')K(t')dt'$ and, consequently, $\delta(t) \to 0$ in the high frequency limit. This ensures that, in the high frequency limit, $P_4^{(ss)}(t)$ in Eq. (31) becomes

$$P_4^{(ss)}(t) = \frac{\langle\chi(t)\rangle}{\langle K(t)\rangle}. \quad (32)$$

The fact that the value of $\delta(t)$ tends to 0 with increase in frequency is also supported by the direct numerical evaluation of $P_4^{(ss)}(t)$ and $\frac{\langle\chi(t)\rangle}{\langle K(t)\rangle}$. One must also note that although the equations (27) and (32) give the steady-state ion-conducting probability, $P_4^{(ss)}(t)$ in compact form, it is not possible to evaluate it analytically as $\chi(t)$ depends on $P_0(t)$, $P_1(t)$, and $P_2(t)$. To determine these probabilities, we resort to numerical solution of the general master equation [Eq. (3)] with time-dependent transition probabilities for oscillating voltage. The numerically determined time-dependent probabilities, $P_n(t)$, are used to obtain the ionic current and entropy production rates for further studies. The details are given in Sec. III.

D. Entropy production rates: Nonequilibrium characterization of ion channel

To explore the nonequilibrium thermodynamic features of the potassium ion channel, here we discuss the entropy production rates due to the channel kinetics. We start from the definition of the entropy of the system in terms of the Shannon entropy as [35,44,45]

$$S_{sys}(t) = -k_B\sum_n P_n(t)\ln P_n(t). \quad (33)$$

Using the master equation, Eq. (3), we get the system entropy production rate (epr) as

$$\dot{S}_{sys}(t) = \frac{1}{2}\sum_{n,\mu=\pm1}[w_\mu(n-\nu_\mu|n)(t)P_{(n-\nu_\mu)}(t) - w_{-\mu}(n|n-\nu_\mu)(t)P_n(t)]\ln\left[\frac{P_{(n-\nu_\mu)}(t)}{P_n(t)}\right], \quad (34)$$

where we set the Boltzmann constant, $k_B = 1$. Here the voltage-dependent transition probabilities are functions of time due to the explicit time dependence of the voltage as given in Eq. (4). We have assumed ideal reservoir (surroundings) with no inherent entropy production except through the boundaries of the system. The system epr can be split as [44–49]

$$\dot{S}_{sys}(t) = \dot{S}_{tot}(t) - \dot{S}_m(t). \quad (35)$$

Here the first term in the right-hand side of Eq. (35) gives the total epr and the second term denotes the medium epr due to the entropy flux into the surroundings. They are defined as

$$\dot{S}_{tot}(t) = \frac{1}{2}\sum_{n,\mu=\pm1}[w_\mu(n-\nu_\mu|n)(t)P_{(n-\nu_\mu)}(t) - w_{-\mu}(n|n-\nu_\mu)(t)P_n(t)] \times \ln\left[\frac{w_\mu(n-\nu_\mu|n)P_{(n-\nu_\mu)}(t)}{w_{-\mu}(n|n-\nu_\mu)P_n(t)}\right] \quad (36)$$

and

$$\dot{S}_m(t) = \frac{1}{2}\sum_{n,\mu=\pm1}[w_\mu(n-\nu_\mu|n)(t)P_{(n-\nu_\mu)}(t) - w_{-\mu}(n|n-\nu_\mu)(t)P_n(t)] \times \ln\left[\frac{w_\mu(n-\nu_\mu|n)}{w_{-\mu}(n|n-\nu_\mu)}\right]. \quad (37)$$

Using the values of forward and backward transition probabilities from Eq. (4) into Eq. (36) and considering the boundary conditions $P_{(n-1)} = 0$ for $n = 0$ and $P_{(n+1)} = 0$ for $n = n_T$, we finally obtain the expression of $\dot{S}_{\rm tot}(t)$ for ion channel as

$$\dot{S}_{\rm tot}(t) = \sum_{n=0}^{n_T-1}[k_1(V(t))(n_T-n)P_n(t) - k_{-1}(V(t))(n+1) \times P_{(n+1)}(t)]\ln\left[\frac{k_1(V(t))(n_T-n)P_n(t)}{k_{-1}(V(t))(n+1)P_{(n+1)}(t)}\right]. \quad (38)$$

In the case where the system attains equilibrium, the total epr becomes zero. When the system reaches a NESS [35,36,50–52] it is characterized by a nonzero total epr [35,36,53].

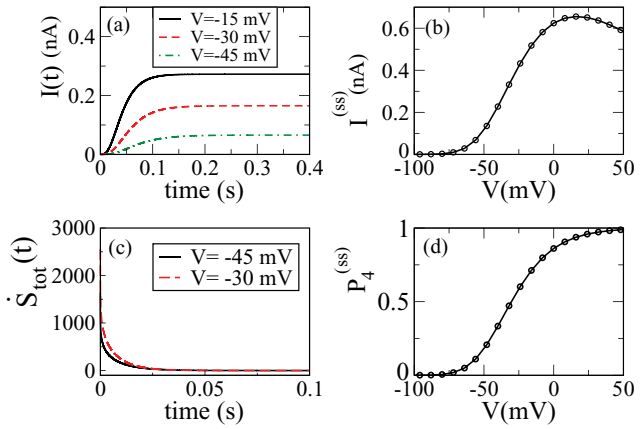

FIG. 1. (Color online) (a) Ionic current, $I(t)$, in nanoamperes (nA) plotted against time (in s) at constant depolarizing voltages, $V = -15$, -30 and -45 mV, respectively. In (b) and (d), the steady-state ionic current, $I^{(ss)}$, and probability of ion-conducting state, $P_4^{(ss)}$, are plotted as a function of voltage at steady state. In (c), the total entropy production rate(epr), $\dot{S}_{\rm tot}(t)$, is plotted as a function of time at depolarizing voltages, $V = -30$ and -45 mV, respectively. At constant voltage, system reaches equilibrium characterized by vanishing total epr.

III. NUMERICAL STUDY OF THE VOLTAGE-GATED *SHAKER* POTASSIUM ION CHANNEL

In this section, using the numerical solution of the master equation given in Eq. (5) for ion channel kinetics with time-dependent voltage, we determine the ionic current (described below) as well as the various entropy production rates with dynamical hysteresis phenomenon. Equation (5) is numerically solved using Heun's algorithm with constant time steps. We have taken the rate parameters from the experimental work of Kargol *et al.* [14] on the *Shaker* potassium ion channel expressed in mammalian cells, tsA 201. The rate constants at zero voltage are taken as $k_1(0) = 124.8\ {\rm s}^{-1}$ and $k_{-1}(0) = 4.74\ {\rm s}^{-1}$. The gating charges associated with both forward and backward transitions rates are $q^+ = 0.66e$ and $q^- = -0.64e$, respectively. The temperature is taken as 12 °C. The externally applied oscillating voltage is considered here as sinusoidal.

In this paper our main aim is to study the case of oscillating voltage. However, for completeness of the study and as a theoretical support of a physiologically important experimental system [14], we first briefly discuss the case of constant voltage where the master equation is analytically solvable.

A. Kinetics and thermodynamics at constant voltage

Experimentally, kinetic description is usually carried out by measuring the ionic current, $I(t)$, which is calculated using the expression

$$I(t) = g_0 g(V)(V - V_r)P_4(t). \quad (39)$$

Here g_0 is the overall scaling factor representing the cell expression rate taken as $g_0 = 1.013$ [14]. The functional form of the nonlinear conductance, $g(V)$ (in microsiemens, μS), is taken from the experimental paper of Kargol *et al.* [15] and given as $g(V) = 1.340 \times 10^{-9}(V)^3 - 7.30 \times 10^{-8}(V)^2 - 3.35 \times 10^{-5}(V) + 4.470 \times 10^{-3}$. V_r is the reversal potential at which no ionic current can pass from the cell and taken here as $V_r = -90$ mV. From Fig. 1(a) it is observed that the ionic current, $I(t)$, first increases with time and then saturates at a constant value. The magnitude of $I(t)$ increases with increase in constant (depolarizing) voltage, V. The variation of conductance, $g(V)$, as a function of voltage, V, is given by an inverted basin passing through a maximum. The probability of ion-conducting state at steady state, $P_4^{(ss)}$, shows a sigmoidal rise with increasing depolarizing voltage and goes to saturation at high (positive) voltage values as is evident from Fig. 1(d). The current at steady state, $I^{(ss)}$, shows similar behavior; however, at high (positive) depolarizing voltages it exhibits a small decay as shown in Fig. 1(b). This is due to the nonlinear voltage dependence of the conductance, $g(V)$. The nature of the current-voltage curve at steady state follows a similar qualitative trend as that of the experimental results of Kargol *et al.* for the voltage clamp study.

To investigate the thermodynamic nature of the steady state at constant voltage, we have calculated the total entropy production rate, $\dot{S}_{\rm tot}(t)$, from Eq. (38). Substituting the time-dependent probability value, $P_n(t)$, from Eq. (6) into Eq. (38), we obtain

$$\dot{S}_{\rm tot}(t) = [k_1(V)\langle n_T - n(t)\rangle - k_{-1}(V)\langle n(t)\rangle]\ln\left[\frac{k_1(V)Y(t)}{k_{-1}(V)X(t)}\right]. \quad (40)$$

Using Eqs. (7) and (8), we obtain the steady-state values of $X(t)$ and $Y(t)$ as $X^{(ss)} = [\frac{k_1(V)}{k_1(V)+k_{-1}(V)}]$ and $Y^{(ss)} = [\frac{k_{-1}(V)}{k_1(V)+k_{-1}(V)}]$. It then follows easily from Eq. (40) that $\dot{S}_{\rm tot}(t)$ becomes zero at equilibrium for a constant external voltage. The analytical result is supported by the numerical result shown in Fig. 1(c).

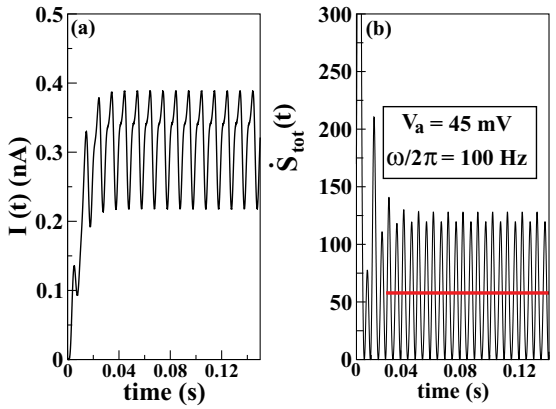

FIG. 2. (Color online) The ionic current, $I(t)$, and entropy production rate, $\dot{S}_{\rm tot}(t)$, are plotted as a function of time. The bold line in (b) denotes the mean value of $\dot{S}_{\rm tot}(t)$ at NESS.

B. Nonequilibrium behavior for oscillating voltage: Dynamic entropy hysteresis

Now we come to the more interesting case of the time-dependent external voltage. We take a sinusoidal voltage variation, $V(t) = V_0 + V_a \sin\omega t$, with mean V_0, amplitude V_a, and frequency ω. We numerically solve the master equation, Eq. (5), to get the probability of the ion-conducting state, $P_4(t)$. The ionic current, $I(t)$, and various entropy production rates are then determined using this probability. The ionic current, $I(t)$, is calculated according to Eq. (39) by considering the time-dependent voltage variation. For oscillating external voltage, the ionic current reaches a time-periodic steady value, $I^{(\rm ss)}(t)$. The steady state is actually a NESS characterized by a nonzero total epr, $\dot{S}_{\rm tot}(t)$, shown in Fig. 2(b). $\dot{S}_{\rm tot}(t)$ oscillates around a nonzero mean value, which is indicated in the figure with a bold line.

In Figs. 3(a) and 3(b), $I^{(\rm ss)}(t)$ vs voltage and $P_4^{(\rm ss)}(t)$ vs voltage plots are shown for three different frequency values (low, medium, and high) of the external voltage at steady state over a period. The hysteresis is evident in both cases and tends to vanish at very low and at very high frequencies with the hysteresis loop area disappearing in these two limits. We want to point out the nature of the $P_4^{(\rm ss)}(t)$-voltage plot specifically at the two limiting situations; at low frequency of the external voltage, $P_4^{(\rm ss)}(t)$ oscillates significantly, whereas at high frequency, the amplitude of the oscillation is much smaller and $P_4^{(\rm ss)}(t)$ deviates the most from its instantaneous steady state (equilibrium) value, i.e., the value $P_4^{(\rm ss)}(t)$ will take if the time-dependent voltage is frozen at the value taken at that instant.

A similar kind of hysteretic behavior is present in the medium epr, $[\dot{S}_m^{(\rm ss)}(t)]$-voltage, and the system epr, $[\dot{S}_{\rm sys}^{(\rm ss)}(t)]$-voltage, plots as shown in Figs. 3(c) and 3(d) at the nonequilibrium steady state for the same frequency values. Apart from the vanishing hysteresis loop area at the limiting situations of low and high frequencies, one can see from these plots that the values of both $\dot{S}_m^{(\rm ss)}(t)$ and $\dot{S}_{\rm sys}^{(\rm ss)}(t)$ tend to zero as $\omega \to 0$ (shown here with $\omega/2\pi = 0.1$ Hz). However, at the high frequency limit, these quantities have finite values although the corresponding hysteresis disappears. The $\dot{S}_m^{(\rm ss)}(t)$-voltage plot becomes highly asymmetric in this limit, whereas the $\dot{S}_{\rm sys}^{(\rm ss)}(t)$-voltage plot is almost symmetric. This amounts to a finite value of total epr, implying that the steady state is a NESS. This is also true for any intermediate frequency value of the external voltage. All the entropy production rates tend to zero and the NESS tends to equilibrium only at the $\omega \to 0$ limit. It is quite obvious that, in the low frequency limit, $P_n^{(\rm ss)}(t)$ tends to its equilibrium value. In this case, the condition of detailed balance is satisfied as in the case of constant voltage. Therefore, at steady state, the total entropy production rate, $\dot{S}_{\rm tot}^{(\rm ss)}(t)$, becomes zero in the low frequency limit.

For a thorough analysis, we have plotted the total epr, $[\dot{S}_{\rm tot}^{(\rm ss)}(t)]$ vs voltage, at the NESS in Fig. 4 at the frequencies

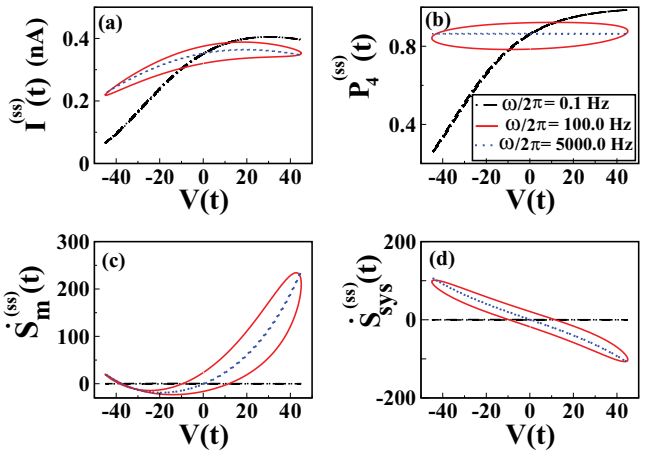

FIG. 3. (Color online) In (a)–(d), ionic current, $I^{(\rm ss)}(t)$, probability of ion conducting state, $P_4^{(\rm ss)}(t)$, medium entropy production rate, $\dot{S}_m^{(\rm ss)}(t)$, and system entropy production rate, $\dot{S}_{\rm sys}^{(\rm ss)}(t)$, are plotted against oscillating voltage (sinusoidal) with frequency $\omega/2\pi = 0.1, 100.0,$ and 5000.0 Hz, respectively, at NESS over a time period. In all cases, hysteretic behavior is observed which vanishes at low and high frequency domains.

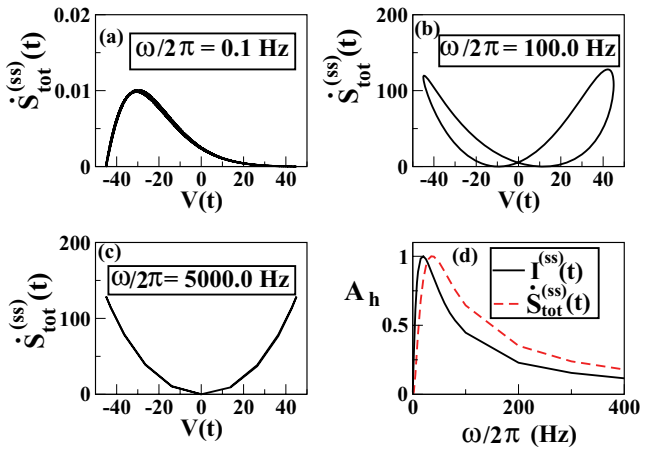

FIG. 4. (Color online) Total entropy production rate, $\dot{S}_{\rm tot}^{(\rm ss)}(t)$, is plotted against oscillating voltage, $V(t)$, at low, medium, and high frequency values at steady state over a time period, depicted in (a), (b), and (c), respectively. In (d), the normalized hysteresis loop area, A_h, of the current-voltage and $\dot{S}_{\rm tot}^{(\rm ss)}(t)$-voltage curves is plotted, which passes through a maximum, indicating that hysteresis is dynamic in nature.

mentioned in Fig. 3. At the low frequency case with the vanishing hysteresis loop area, $\dot{S}_{\rm tot}^{\rm (ss)}(t)$ becomes almost zero at the extremum points of the voltage, $V_e = \pm V_a (= \pm 45$ mV) as shown in Fig. 4(a). Hence, at these two points the system is only infinitesimally away from the equilibrium. Now at very low frequency with extremely slow voltage variation, the system can always adjust to the instantaneous value of the voltage. Hence, one can roughly picturize the points $V_e = \pm 45$ mV as the classical turning points of a simple pendulum where the pendulum becomes stationary momentarily. With the increase in the frequency of $V(t)$, the response of the system to the external driving starts to lag behind. This is reflected in the plot with $\omega/2\pi = 100$ Hz in Fig. 4(b), where $\dot{S}_{\rm tot}^{\rm (ss)}(t)$ becomes close to zero at points $0 < |V_e| < V_a$. At $\omega \to \infty$, the system totally fails to sense the ultrafast voltage variation and sees only the average voltage value, V_0. In this limiting case, the two points mentioned above merge at $V_e = V_0 = 0$ mV as shown in Fig. 4(c) for $\omega/2\pi = 5000$ Hz. We have also shown the variation of the hysteresis loop area, A_h for the $\dot{S}_{\rm tot}^{\rm (ss)}(t)$-voltage as well as the current-voltage hysteresis plots in Fig. 4(d) at the NESS. The $\dot{S}_{\rm tot}^{\rm (ss)}(t)$-voltage and current-voltage hysteresis loop areas are calculated numerically by integrating the value of $\dot{S}_{\rm tot}^{\rm (ss)}(t)$ and $I^{\rm (ss)}(t)$ over a complete period of oscillating voltage, $V(t)$ according to the formula [54] $A_h = \oint \alpha(V(t))dV$. Here α is $\dot{S}_{\rm tot}^{\rm (ss)}(t)$ or $I^{\rm (ss)}(t)$. It is clear that the hysteresis loop areas for the two plots maximize at close but different frequency values, whereas at $\omega \to 0$ as well as at $\omega \to \infty$ limits, both the hysteresis loop areas go to zero. Therefore, the hysteresis observed in $\dot{S}_{\rm tot}^{\rm (ss)}(t)$-voltage and $I^{\rm (ss)}(t)$-voltage curves are dynamic in nature. Interestingly, a close inspection of the $\dot{S}_{\rm tot}^{\rm (ss)}(t)$-voltage plot reveals that these two frequency limits of vanishing hysteresis differ thermodynamically, as evident from the variation of total epr with $V(t)$. For the $\omega \to 0$ limit, the amplitude of $\dot{S}_{\rm tot}^{\rm (ss)}(t)$ tends to zero as already mentioned, whereas, in the $\omega \to \infty$ limit, its amplitude tends to a finite value.

For more clarification of the above statement, we have plotted the average total epr over a time period, $\langle \dot{S}_{\rm tot}^{\rm (ss)}(t) \rangle$, in Fig. 5(a) at NESS as a function of the frequency of the external voltage. Here the average is defined as $\langle \dot{S}_{\rm tot}^{\rm (ss)}(t) \rangle = \frac{1}{T}\int_0^T \dot{S}_{\rm tot}^{\rm (ss)}(t)dt$. From the figure, one can see that the average total epr increases steadily from zero at very low frequency to saturation at high frequency values. Therefore, the nonequilibrium steady state reached by the system is infinitesimally close to equilibrium at the $\omega \to 0$ limit, whereas it is farthest from equilibrium at the $\omega \to \infty$ limit for the given parameters of the model system and the amplitude of the external voltage. This plot clearly shows that the low and high frequency limits associated with vanishing hysteresis are indeed thermodynamically distinct. Furthermore, in Fig. 5(b), we have plotted the average current over a period, $\langle [I^{\rm (ss)}(t)]_{\rm sc} \rangle$ versus frequency at different voltage amplitudes. Here the "sc" superscript indicates that the ionic current is scaled with the nonlinear conductance, $g(v)$. The functional form of $g(V)$ is generally an experimentally determined equation that can vary from experiment to experiment. So to obtain the general behavior of the ionic current we have calculated the scaled current. From Fig. 5(b), it is observed that the average ionic

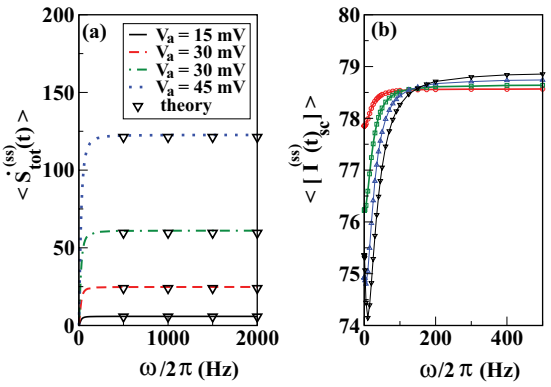

FIG. 5. (Color online) (a) Average entropy production rate over a period, $\langle \dot{S}_{\rm tot}^{\rm (ss)}(t) \rangle$, is plotted against frequency, $\omega/2\pi$, with amplitude, $V_a = 15, 30, 45$, and 60 mV. The value of $\langle \dot{S}_{tot}^{(ss)}(t) \rangle$ saturates at higher frequency values. (b) $\langle [I^{\rm (ss)}(t)]_{\rm sc} \rangle$ indicates the ionic current over a period scaled with $g(v)$ and is plotted against frequency, $\omega/2\pi$, with the same amplitudes. With increasing the amplitude values, $\langle [I^{\rm (ss)}(t)]_{\rm sc} \rangle$ becomes almost constant in the high frequency; however, $\langle \dot{S}_{\rm tot}^{\rm (ss)}(t) \rangle$ increases with increase in the value of amplitude, V_a. We have also plotted the values of $\langle \dot{S}_{\rm tot}^{\rm (ss)}(t) \rangle$ in the high frequency limit ($\omega \to \infty$) obtained from Eq. (41) at various amplitudes denoted with the label "theory" and compared with the numerical results.

current, $\langle [I^{\rm (ss)}(t)]_{\rm sc} \rangle$, increases to saturation with increase in the frequency value. It can be seen from Fig. 5(b) that in the high frequency limit, $\langle [I^{\rm (ss)}(t)]_{\rm sc} \rangle$ becomes almost independent of amplitude. However, from Fig. 5(a) it is evident that the high frequency limiting value of $\langle \dot{S}_{\rm tot}^{\rm (ss)}(t) \rangle$ increases sharply with increasing amplitude. In Fig. 5(a) we have also shown this limiting value of $\langle \dot{S}_{\rm tot}^{\rm (ss)}(t) \rangle$ in the high frequency limit ($\omega \to \infty$) obtained from the analytical expression given below

$$\dot{S}_{\rm tot}^{\rm (ss)}(t) = n_T \left[\frac{k_1(0)k_{-1}(0)2\sinh(V'(t))}{k_1(0) + n_T k_{-1}(0)} \right] 2V'(t). \quad (41)$$

Here $V'(t) = xV(t)$ with $x = \frac{q}{k_B T'}$. For details of the derivation see the Appendix.

For a clear understanding of the amplitude dependence of $\langle \dot{S}_{\rm tot}^{\rm (ss)}(t) \rangle$ and $\langle [I^{\rm (ss)}(t)]_{\rm sc} \rangle$, we have plotted these quantities as a function of V_a^2 for low, medium, and high frequency values at NESS, shown in Fig 6. For oscillating voltage, V_a^2 is proportional to the energy supplied to the system and $\dot{S}_{\rm tot}$ is a measure of dissipative flux from the system. From Figs. 6(a) and 6(c) it is observed that, at low and medium frequencies, $\langle [I^{\rm (ss)}(t)]_{\rm sc} \rangle$ increases with an increase in the value of V_a^2 after passing through a minimum. Such behavior is generated due to the determination of the current from Eq. (39). However, at the high frequency limit, this tendency vanishes and $\langle [I^{\rm (ss)}(t)]_{\rm sc} \rangle$ saturates with increase in the value of V_a^2 which is shown in Fig. 6(c). In Figs. 6(b), 6(d), and 6(f), we have plotted $\langle \dot{S}_{\rm tot}^{\rm (ss)}(t) \rangle$ as a function of V_a^2 at low, medium, and high frequencies, respectively. From close inspection, one can observe an interesting difference among the variations of $\langle [I^{\rm (ss)}(t)]_{\rm sc} \rangle$ and $\langle \dot{S}_{\rm tot}^{\rm (ss)}(t) \rangle$ as a function of V_a^2. In the low and medium frequency regions, $\langle [I^{\rm (ss)}(t)]_{\rm sc} \rangle$ continues increasing with V_a^2, whereas $\langle \dot{S}_{\rm tot}^{\rm (ss)}(t) \rangle$ increases to a saturation. This is evident from Figs. 6(a)–6(d). However, in the high frequency limit the situation gets reversed, as shown

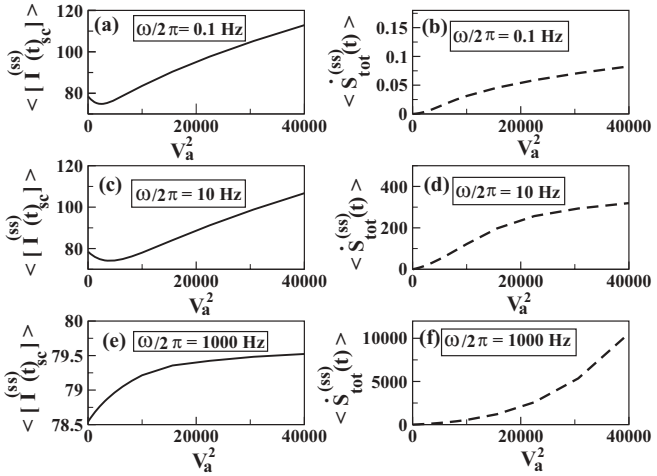

FIG. 6. In (a), (c), and (e), the average ionic current over a period at steady state, $\langle [I^{(ss)}(t)]_{sc} \rangle$, is plotted against square of the amplitude, V_a^2 at low ($\omega/2\pi = 0.1$ Hz), medium ($\omega/2\pi = 10$ Hz), and high frequency ($\omega/2\pi = 1000$ Hz), respectively. Average entropy production rate over a period at steady state, $\langle \dot{S}_{tot}^{(ss)}(t) \rangle$, is plotted against V_a^2 with the same frequency values which are depicted in (b), (d), and (f), respectively.

in Figs. 6(e) and 6(f). Here $\langle \dot{S}_{tot}^{(ss)}(t) \rangle$ increases nonlinearly with V_a^2 but $\langle [I^{(ss)}(t)]_{sc} \rangle$ ultimately saturates. So the steep rise of the dissipation function with the input power is associated with a limiting ionic current. On the other hand, when the dissipation function gets saturated, the current increases almost linearly as a function of input power. Hence, the fraction of input energy that goes out from the system as unavailable energy governs the efficiency of the ion conduction.

We report another intriguing observation. We have plotted the ionic current, $I^{(ss)}(t)$, the total entropy production rate, $\dot{S}_{tot}^{(ss)}(t)$, and $V(t)$ at high frequency, $\omega/2\pi = 5000$ Hz, over a period at steady state in Fig. 7. From Fig. 7(b), it is observed that in the high-frequency regime, $\dot{S}_{tot}^{(ss)}(t)$ oscillates with a time period which is half of the external voltage, $V(t)$. However,

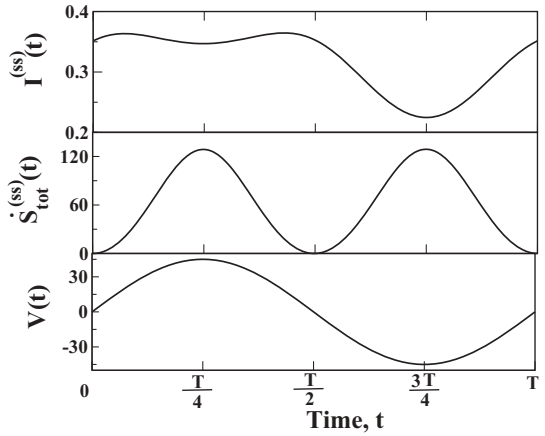

FIG. 7. The ionic current, $I^{(ss)}(t)$, total entropy production rate, $\dot{S}_{tot}^{(ss)}(t)$, and oscillating voltage, $V(t)$, are plotted with time at $\omega/2\pi = 5000$ Hz over an oscillation period at NESS. The time required to complete an oscillation cycle is the same for $I^{(ss)}(t)$ but half for $\dot{S}_{tot}^{(ss)}(t)$ compared to that of voltage, $V(t)$.

the time period of ionic current, $I^{(ss)}(t)$, is the same as that of the external voltage, which is depicted in Fig. 7(a). Now, from Eq. (41), it can be easily shown that $\dot{S}_{tot}^{(ss)}(t) = \dot{S}_{tot}^{(ss)}(t + T/2)$, where T is the period of the external voltage. For a detailed derivation see the Appendix. Hence, at the high frequency limit, the total epr at NESS oscillates with a frequency which is double of that of the external voltage.

Before concluding, we discuss how the single ion channel results can be extended for L_T number of *Shaker* channels. In Eq. (1), we have already discussed the kinetic scheme of a single ion channel, where an ion channel remains in any one of the five conformational states (C_0 to C_4) at a particular instant of time. For L_T number of channels, the kinetic scheme can be written as [9]

$$m_0 \underset{W(m_1|m_0)(t)}{\overset{W(m_0|m_1)(t)}{\rightleftharpoons}} m_1 \underset{W(m_2|m_1)(t)}{\overset{W(m_1|m_2)(t)}{\rightleftharpoons}} m_2 \underset{W(m_3|m_2)(t)}{\overset{W(m_2|m_3)(t)}{\rightleftharpoons}} m_3 \underset{W(m_4|m_3)(t)}{\overset{W(m_3|m_4)(t)}{\rightleftharpoons}} m_4, \tag{42}$$

where the transition probabilities are given as $W(m_n|m_{(n-1)})(t) = m_n w_{-1}(n|n-1)(t)$ and $W(m_{(n-1)}|m_n)(t) = m_{(n-1)} w_1(n-1|n)(t)$. Here $w_{-1}(n|n-1)(t)$ and $w_1(n-1|n)(t)$ are defined as in Eq. (4). Here m_n specifies the number of channels in the C_n conformational state (n varies from 0 to 4) at time t with $\sum_{n=0}^{4} m_n = L_T$. The corresponding master equation can be written as [9]

$$\begin{aligned}\frac{\partial Q(\mathbf{m},t)}{\partial t} &= \sum_{n=1}^{4} (m_n + 1) w_{-1}(n|n-1)(t) Q(m_{(n-1)} - 1, m_n + 1, t) \\ &\quad + (m_{(n-1)} + 1) w_1(n-1|n)(t) Q(m_{(n-1)} + 1, m_n - 1, t) \\ &\quad - m_n w_{-1}(n|n-1)(t) Q(\mathbf{m},t) - m_{(n-1)} w_1(n-1|n)(t) \\ &\quad \times Q(\mathbf{m},t).\end{aligned} \tag{43}$$

Here $Q(\mathbf{m},t)$ is the probability of having the population state vector $\mathbf{m}$ at time t where $\mathbf{m} \equiv (m_1, m_2, m_3, m_4)$ with $m_0 = L_T - \sum_{n=1}^{4} m_n$. For analytical simplicity, we have considered the two-state Markov model instead of a five-state one by assuming that all the ion channels are in either the inactive or active state. Therefore, for the two-state Markov model, the kinetic scheme can be written as

$$\text{closed} \underset{k_{-1}(V(t))}{\overset{k_1(V(t))}{\rightleftharpoons}} \text{open}. \tag{44}$$

These "closed" and "open" states are similar to the conformational states m_0 and m_4 in Eq. (42), where all the subunits in an ion channel remain in inactive and active states, respectively. For this two-state case, the master equation can be constructed in terms of the number of channels in the open state at a particular instant of time as

$$\begin{aligned}\frac{dQ(m,t)}{dt} &= k_1(V(t))(L_T - m + 1) Q(m-1,t) \\ &\quad + k_{-1}(V(t))(m+1) Q(m+1,t) \\ &\quad - k_1(V(t))(L_T - m) Q(m,t) - k_{-1}(V(t)) m \\ &\quad \times Q(m,t).\end{aligned} \tag{45}$$

Here $Q(m,t)$ is the probability of having m number of channels in the open state at time t where the total number of channels, L_T is arbitrary. The master equation described in Eq. (45) looks similar to that in Eq. (5) for a single ion channel consisting of five conformational states. At constant voltage, solution of Eq. (45) becomes a binomial distribution as described in Eq. (6) and the average number of channels in open state is given by $\langle m(t)\rangle = L_T X(t)$, where $X(t)$ is defined similarly as in Eq. (7). At steady state, the value of $X(t)$ becomes $X^{(\mathrm{ss})} = \frac{k_1(V)}{k_1(V)+k_{-1}(V)}$ and the probability distribution becomes $Q^{(\mathrm{ss})}(m) = \frac{L_T!}{m!(L_T-m)!}(X^{(\mathrm{ss})})^m(Y^{(\mathrm{ss})})^{L_T-m}$. If L_T is very large and $X^{(\mathrm{ss})}$ is very small, $\frac{L_T!}{(L_T-m)!}$ becomes $(L_T)^m$ and $(1-X^{(\mathrm{ss})})^{(L_T-m)} \approx \exp(-X^{(\mathrm{ss})}L_T)$. The probability distribution then becomes Poissonian,

$$Q^{(\mathrm{ss})}(m) = \frac{(L_T X^{(\mathrm{ss})})^m}{m!}\exp(-X^{(\mathrm{ss})}L_T), \tag{46}$$

where $X^{(\mathrm{ss})}L_T$ is the average number of ion channels in the open state. At a particular time, t, the ionic current can be calculated as

$$I(t) = g_0 g(V)(V-V_r)\langle m(t)\rangle = g_0 g(V)(V-V_r)L_T Q_o(t), \tag{47}$$

where $Q_o(t)$ is the open state probability of a single channel for the two-state case and the other parameters carry similar meanings, as described in Sec. III A. From the numerical analysis of Eq. (45), we can also obtain the total epr, $\dot{S}_{\mathrm{tot}}(t)$, and other nonequilibrium thermodynamic quantities.

IV. CONCLUSION

In view of the physiological significance of the hysteretic response, here we have given a nonequilibrium thermodynamic description of a voltage-gated potassium ion channel using the stochastic master equation approach. Starting from an experimentally proposed five-state Markov process of a *Shaker* potassium ion channel, the traditional single-parameter Hodgkin-Huxley equation is shown to be connected with the master equation corresponding to the stochastic transitions between the five conformational states at fixed voltage. The powered Boltzmann distribution of the steady-state probability of the ion-conducting state is also obtained from the master equation in this case. Now from thermodynamic analysis it is observed that, for constant external voltage, the system reaches equilibrium, indicated by the vanishing total entropy production rate.

For oscillating voltage, the current as well as the entropy production rates show dynamic hysteresis with vanishing area of hysteresis loop for very low and very high frequencies of the external voltage. However, by analyzing the total entropy production rate we have shown that the two limiting situations differ thermodynamically. At the very low frequency limit, the system remains close to equilibrium, whereas, at high frequency, it goes far away from equilibrium, associated with a finite amount of dissipation. To find the efficiency of the ion current production, the NESS is characterized by the nonlinear dependence of the dissipation function on the power of the external field. A strong nonlinear variation of the unavailable energy flux with the input power dictates that an optimum limit of frequency of the oscillating voltage is necessary for a reasonable steady ionic current to appear. Another intriguing aspect is that the total entropy production rate oscillates at NESS with half of the time period of the external voltage in the limit of high frequency. We have also discussed the extension of the present analysis to multiple ion channels, which is easier to tackle experimentally. The nonequilibrium thermodynamic analysis done here for a potassium ion channel is also generically valid for other Markov processes of similar ion conduction problems, namely sodium ion channels, ryanodine receptor, and IP_3 receptors [43].

ACKNOWLEDGMENT

K.B. acknowledges the Council of Scientific and Industrial Research (C.S.I.R.), India, for partial financial support as a Senior Research Fellow.

APPENDIX: ESTIMATION OF TOTAL ENTROPY PRODUCTION RATE AT HIGH FREQUENCY LIMIT AT NESS

Here we have estimated the entropy production rate in the high frequency limit from Eq. (38) at NESS. From numerical analysis it is observed that for the parameters $k_1(0)$ and $k_{-1}(0)$ considered in the text, the steady-state values of $P_0(t)$, $P_1(t)$, and $P_2(t)$ tend to zero. Therefore, $\chi(t)$ in Eq. (14) can be written as $\chi(t) \approx k_1(V(t))$ and $\dot{S}_{\mathrm{tot}}^{(\mathrm{ss})}(t)$ in Eq. (38) can be expressed in terms of the steady-state probability of ion-conducting state, $P_4^{(\mathrm{ss})}(t)$, as

$$\dot{S}_{\mathrm{tot}}^{(\mathrm{ss})}(t) = \left[k_1(V(t))\left(1-P_4^{(\mathrm{ss})}(t)\right) - k_{-1}(V(t))n_T P_4^{(\mathrm{ss})}(t)\right] \times \ln\frac{k_1(V(t))\left(1-P_4^{(\mathrm{ss})}(t)\right)}{k_{-1}(V(t))n_T P_4^{(\mathrm{ss})}(t)}. \tag{A1}$$

In the high frequency limit, the steady-state value of $\dot{S}_{\mathrm{tot}}^{(\mathrm{ss})}$ can be easily calculated by substituting the value of $P_4^{(\mathrm{ss})}(t)$ from Eq. (32) into Eq. (A1), whereby we get

$$\dot{S}_{\mathrm{tot}}^{(\mathrm{ss})}(t) = n_T\left[\frac{k_1(V(t))\langle k_{-1}(V(t))\rangle - k_{-1}(V(t))\langle k_1(V(t))\rangle}{\langle K(t)\rangle}\right] \times \ln\frac{k_1(V(t))\langle k_{-1}(V(t))\rangle}{k_{-1}(V(t))\langle k_1(V(t))\rangle}. \tag{A2}$$

Here $K(t) = k_1(V(t)) + n_T k_{-1}(V(t))$. When $\omega \to \infty$, $\langle k_1(V(t))\rangle$ and $\langle k_{-1}(V(t))\rangle$ can be written as

$$\langle k_1(V(t))\rangle = f_1 k_1(0)$$

and

$$\langle k_{-1}(V(t))\rangle = f_{-1}k_{-1}(0), \tag{A3}$$

where $f_1 = \langle\exp[x_1 V(t)]\rangle$ with $x_1 = \frac{q^+}{k_B T'}$ and $f_{-1} = \langle\exp[x_{-1}V(t)]\rangle$ with $x_{-1} = \frac{q^-}{k_B T'}$. As in the main text, for the value of $q^+ \approx -q^-$, we have taken $q^+ = q^- = q$. So we can write $x_1 = x$ and $x_{-1} = -x$. Therefore, $f_{\pm 1}$ can be written as

$$f_{\pm 1} = 1 \pm \langle x V(t)\rangle + \frac{(\langle x V(t)\rangle)^2}{2} \pm \frac{(\langle x V(t)\rangle)^3}{3!} + \cdots,$$

where $\langle xV(t)\rangle = \frac{1}{T}\int_0^T xV_0\sin(\omega t)dt$. When n is odd, $\langle xV(t)\rangle^n = 0$ and for even values of n, $\langle xV(t)\rangle^n$ becomes independent of frequency, ω. Hence, we can write $\langle k_1(V(t))\rangle = fk_1(0)$ and $\langle k_{-1}(V(t))\rangle = fk_{-1}(0)$, where $f_{\pm 1} = f$. Using these relations, Eq. (A2) can be written as

$$\dot{S}_{\rm tot}^{(\rm ss)}(t) = n_T\left[\frac{k_1(0)k_{-1}(0)2\sinh(V'(t))}{k_1(0)+n_Tk_{-1}(0)}\right]2V'(t), \quad \text{(A4)}$$

where $V'(t) = xV(t)$ with $x = \frac{q}{k_BT'}$.

It can be easily shown that in the high frequency limit, $\dot{S}_{\rm tot}^{(\rm ss)}(t)$ oscillates with a time period which is half of that of the external voltage, $V(t)$. To prove this, first, we note that $V(t+\frac{T}{2}) = V_a\sin\omega(t+\frac{T}{2}) = -V_a\sin\omega t = -V(t)$ and, thus, $\sinh V'(t+\frac{T}{2})] = -\sinh(V'(t))$. It then follows from Eq. (A4) that

$$\dot{S}_{\rm tot}^{(\rm ss)}\left(t+\frac{T}{2}\right) = n_T\left[\frac{k_1(0)k_{-1}(0)2\sinh\left[V'\left(t+\frac{T}{2}\right)\right]}{k_1(0)+n_Tk_{-1}(0)}\right] \times 2V'\left(t+\frac{T}{2}\right) = \dot{S}_{\rm tot}^{(\rm ss)}(t). \quad \text{(A5)}$$

Therefore, in the high frequency limit, $\dot{S}_{\rm tot}^{(\rm ss)}(t)$ versus the time curve becomes symmetric and it completes a cycle at $T/2$.

[1] D. L. Nelson and M. M. Cox, *Lehninger Principles of Biochemistry*, 4th ed. (Worth, New York, 2004).
[2] G. M. Shepherd, *Neurobiology*, 3rd ed. (Oxford University Press, Oxford, 1994).
[3] A. L. Hodgkin and A. F. Huxley, J. Physiol. **117**, 500 (1952).
[4] B. Sakmann and E. Neher, *Single-Channel Recording*, 2nd ed. (Plenum Press, New York, 1995).
[5] F. Bezanilla, IEEE Transact. Nanobiosci. **4**, 34 (2005).
[6] W. N. Zagotta, T. Hoshi, and R. W. Aldrich, J. Gen. Physiol. **103**, 321 (1994).
[7] W. N. Zagotta, T. Hoshl, J. Dittman, and R. W. Aldrich, J. Gen. Physiol. **103**, 279 (1994).
[8] T. Hoshi, W. N. Zagotta, and R. W. Aldrich, J. Gen. Physiol. **103**, 249 (1994).
[9] R. F. Fox and Y. N. Lu, Phys. Rev. E **49**, 3421 (1994).
[10] Y. Pichon, L. Prime, P. Benquet, and F. Tiaho, Eur. Biophys. J. **33**, 211 (2004).
[11] O. Yifrach, Biophys. J. **87**, 822 (2004).
[12] M. M. Millonas and D. A. Hanck, Phys. Rev. Lett. **80**, 401 (1998).
[13] M. M. Millonas and D. A. Hanck, Biophys. J. **74**, 210 (1998).
[14] A. Kargol, A. Hosein-Sooklal, L. Constantin, and M. Przestalski, Gen. Physiol. Biophys. **23**, 53 (2004).
[15] A. Kargol and K. Kabza, Phys. Biol. **5**, 026003 (2008).
[16] M. C. Menconi, M. Pellegrini, M. Pellegrino, and D. Petracchi, Eur. Biophys. J. **27**, 299 (1998).
[17] G. Bertotti and I. D. Mayergoyz, *The Science of Hysteresis: Mathematical Modeling and Applications*, 1st ed. (Academic Press, San Diego, CA, 2006).
[18] C. N. Luse and A. Zangwill, Phys. Rev. E **50**, 224 (1994).
[19] Y. L. He and G. C. Wang, Phys. Rev. Lett. **70**, 2336 (1993).
[20] B. K. Chakrabarty and M. Acharyya, Rev. Mod. Phys. **71**, 847 (1999).
[21] M. C. Mahato and S. R. Shenoy, Phys. Rev. E **50**, 2503 (1994).
[22] B. Hille, *Ion Channels in Excitable Membrane*, 3rd ed. (Sinauer Associates Inc., Sunderland, MA, 2001).
[23] W. Zhou, F. S. Cayabyab, P. S. Pennefather, L. C. Schlichter, and T. E. DeCoursey, J. Gen. Physiol. **111**, 781 (1998).
[24] D. Fologea, E. Krueger, Y. I. Mazur, C. Stith, R. Henry, Y. Okuyama, and G. J. Salamo, Biomembranes **1808**, 12 (2011).
[25] R. Mannikko, S. Pandey, H. P. Larsson, and F. Elinder, J. Gen. Physiol. **125**, 305 (2005).
[26] M. A. Pustovoit, A. M. Berezhkovskii, and S. M. Bezrukov, J. Chem. Phys. **125**, 194907 (2006).
[27] T. Andersson, Math. Biosci. **226**, 16 (2010).
[28] Y. Jiang, A. Lee, J. Chen, V. Ruta, M. Cadene, B. T. Chait, and R. MacKinnon, Nature **423**, 33 (2003).
[29] A. Nekouzadeh, J. R. Silva, and Y. Rudy, Biophys. J. **95**, 3510 (2008).
[30] L. M. Mannuzzu, M. M. Moronne, and E. Y. Isacoff, Science **271**, 213 (1996).
[31] W. R. Silverman, B. Roux, and D. M. Papazian, Proc. Natl. Acad. Sci. USA **100**, 2935 (2003).
[32] J. P. Keener, J. Math. Biol. **58**, 447 (2009).
[33] I. Goychuk and P. Hanggi, Physica A **325**, 9 (2003).
[34] B. Das and G. Gangopadhyay, J. Chem. Phys. **132**, 135102 (2010).
[35] K. Banerjee, B. Das, and G. Gangopadhyay, J. Chem. Phys. **136**, 154502 (2012).
[36] D. Andrieux and P. Gaspard, J. Chem. Phys. **121**, 6167 (2004).
[37] P. Gaspard, J. Chem. Phys. **120**, 8898 (2004).
[38] J. P. Keener, J. Math. Biol. **60**, 473 (2010).
[39] T. L. Hill, J. Chem. Phys. **54**, 34 (1971).
[40] L. W. Shapiro and D. Zeilberger, J. Math. Biol. **15**, 351 (1982).
[41] T. L. Hill, *Cooperativity Theory in Biochemistry-Steady-State and Equilibrium Systems* (Springer-Verlag, New York, 1985).
[42] N. Bindslev, *Drug-cceptor Interactions: Modeling Theoretical Tools to Test and Evaluate Experimental Equilibrium Effects*, 1st ed. (Co-Action Publishing, Sweden, 2008).
[43] J. P Keener and J. Sneyd*Mathematical Physiology*, 1st ed. (Springer, New York, 1998).
[44] L. Jiu-li, C. Van den Broeck, and G. Nicolis, Z. Phys. B **56**, 165 (1984).
[45] G. Nicolis and I. Prigogine, *Self-Organization in Nonequilibrium Systems*, 1st ed. (Wiley, New York, 1977).
[46] G. Nicolis and I. Prigogine, Proc. Natl. Acad. Sci. USA **68**, 2102 (1971).
[47] G. Nicolis, J. Stat. Phys. **6**, 195 (1972).
[48] M. Malek-Mansour and G. Nicolis, J. Stat. Phys. **13**, 197 (1975).
[49] J. Schnakenberg, Rev. Mod. Phys. **48**, 571 (1976).
[50] H. Qian and E. L. Elson, Biophys. Chem. **101**, 565 (2002).
[51] W. Min, L. Jiang, J. Yu, S. C. Kou, H. Qian, and X. S. Xie, Nano Lett. **5**, 2373 (2005).
[52] H. Qian, Annu. Rev. Phys. Chem. **58**, 113 (2007).
[53] M. Vellela and H. Qian, J. R. Soc. Interface **39**, 925 (2009).
[54] M. Das, D. Mondal, and D. S. Ray, J. Chem. Phys. **136**, 114104 (2012).